Heat Capacity Study of Isotactic Polystyrene: Dual Reversible Crystal Melting and Relaxation of Rigid Amorphous Fraction

ARTICLE *in* MACROMOLECULES · MARCH 2004

Impact Factor: 5.8 · DOI: 10.1021/ma035961n

Heat Capacity Study of Isotactic Polystyrene: Dual Reversible Crystal Melting and Relaxation of Rigid Amorphous Fraction

Hui Xu and Peggy Cebe*

Department of Physics and Astronomy, Tufts University, Medford, Massachusetts 02155

Received December 19, 2003; Revised Manuscript Received February 13, 2004

ABSTRACT: Isotactic polystyrene (iPS) is demonstrated to have unique thermal behavior, showing dual reversible crystal melting and irreversible enthalpic relaxation of its rigid amorphous fraction (RAF). Quasi-isothermal temperature-modulated differential scanning calorimetry (TMDSC) and standard DSC were used to study the heat capacity of cold-crystallized iPS. IPS shows two or three endotherms depending upon cold crystallization temperature, T_c. Crystal melting causes the higher temperature endotherm(s), and under quasi-isothermal conditions, we report for the first time observation of dual locally reversible melting endotherms. Quasi-isothermal TMDSC shows that the RAF is established at the crystallization temperature in iPS. Furthermore, we show that the lowest temperature endothermic peak, called the annealing peak, represents the transition of the RAF. For cold-crystallized iPS the annealing peak is an irreversible, enthalpy-involved relaxation of RAF, which transforms solidlike RAF into liquidlike mobile amorphous fraction. Depending upon T_c, RAF may be the sole contributor to the lowest temperature endotherm. To accommodate the relaxation of RAF, the experimentally determined heat capacity should be written in terms of the underlying linear baseline heat capacity plus the enthalpic terms relating to crystal melting and to relaxation of RAF.

Introduction

Recently, a unique experimental technique, called quasi-isothermal temperature-modulated differential scanning calorimetry (TMDSC), has been developed to study reversible melting of polymers.[1−6] Before melting of a molecule from the surface of a crystal is completed, some part bigger or equal to a molecular nucleus may remain attached (crystallized), so that melting and crystallization were shown to be locally reversible within a fraction of a degree.[7] Macromolecular nucleation, a term introduced by Wunderlich et al.,[8] was shown to be involved in segregation of molecular lengths below the equilibrium or zero-entropy-production, melting temperature of the separated fraction. Macromolecular nucleation has a higher free energy barrier than secondary nucleation, and it may lead to independent patches of each molecule on the crystal surface.[8] Wunderlich et al.[9] suggested that the tie macromolecules, which are intercrystalline links, cannot be extracted from the crystal surface until the crystal with high perfection was completely dissolved. Tie molecules, which are attached to the crystals, are suggested to be responsible for the reversible melting of polymers.[7] If the crystal is incompletely melted, the tie molecules act as nuclei for reversible crystallization and melting, without the need of molecular nucleation for crystallization.[7] The observations of quasi-isothermal TMDSC support the suggestion that there is reversible melting in polymer systems on a molecular or submolecular length scale.[1,7]

In the present work, we apply the techniques of quasi-isothermal TMDSC and standard DSC to study multiple melting in cold-crystallized isotactic polystyrene (iPS). First, we use quasi-isothermal TMDSC to investigate the possibility of reversible melting in iPS, which exhibits multiple endotherms in standard DSC. Second, we investigate the lowest endotherm, occurring just above the cold crystallization temperature, and show that it results from enthalpic relaxation of the rigid amorphous fraction.

Interpretation of multiple endotherms in semicrystalline polymers has been a long-standing issue for thermal analysts. In polymers where there is a single crystallographic form, multiple endotherms may arise because of dual crystal populations existing prior to the thermal scan; the lower endotherm is due to melting of thinner lamellae.[10−13] A second possibility is the melting−recrystallization−remelting of a single-crystal population during the thermal scan.[14−18] IPS is one such polymer, showing multiple endotherms dependent upon prior thermal treatment.[14,15,19−25] Because of its relatively slow crystallization rate[15] and high glass transition (T_g = 100 °C),[26] iPS can be quenched to form an amorphous glass. Cold crystallization by heating above T_g results in thermal scans showing two or three endotherms,[14,15,25] which have been interpreted variously by the recrystallization model[15] or dual crystal population model.[14]

Liu and Peterman[27] recently suggested a different mechanism of melting for cold-crystallized iPS. A transmission electron microscopy study[27] revealed that (1) no crystals were observed to melt as the lowest temperature endotherm, at temperature T_a (called the annealing peak), was exceeded; (2) lamellae appeared to become broken, and sections of them melted at the intermediate endotherm (at T_{m1}); (3) broken lamellae "reconnected" between T_{m1} and T_{m2}, which appeared as an exothermic peak in the DSC scan; and (4) remaining parts of the lamellae melted at the uppermost endotherm (at T_{m2}). The authors suggested that crystal perfection varied within a single lamella,[27] a result suggested by their earlier work.[28] There is a distribution of two distinct lamellar components (less perfect and more perfect) with different thermal stabilities existing within a single lamella.[27] The less perfect lamellar domains melt first to form endotherm T_{m1}, while the higher melting peak T_{m2} is mainly due to the melting of a more perfect part within the same lamella but may

* Corresponding author. E-mail peggy.cebe@tufts.edu.

10.1021/ma035961n CCC: $27.50
Published on Web 03/23/2004

also be due, to some lesser extent, to the melting of a recrystallized population during the heating process.[27] In this work, we use quasi-isothermal TMDSC to show for the first time *dual reversible melting* behavior of iPS is associated with the uppermost endotherms.

Another important aspect of this work is to investigate the formation and relaxation behavior of rigid amorphous fraction in iPS by thermal analysis. The relaxation strength at the glass transition (T_g) shows a significant reduction from what is predicted on the basis of the mobile amorphous fraction deduced from a two-phase model. The introduction of rigid amorphous fraction, which is noncrystalline, but does not contribute to the glass transition, allows a good description of polymer relaxation behavior.[29−32] Previous dielectric work by our group showed that RAF was associated with the crystal amorphous interphase in poly(ether ether ketone), PEEK, and poly(phenylene sulfide), PPS.[33,34] In PPS we showed that RAF, created at the cold-crystallization temperature, could be relaxed upon brief heating to a temperature above the lowest crystal melting endotherm.[35] Enthalpic relaxation of RAF was determined to be a measurable (albeit small) contribution to the lowest melting endotherm in PPS.[35]

The formation and relaxation behavior of RAF depend on the polymer under study. In poly(ethylene terephthalate), PET, Song showed that the relaxation of RAF occurs between the glass transition and the premelting peak, which is the lowest endotherm.[36] For poly(phenylene oxide), PPO, Wunderlich et al.[37] found that the RAF could only be relaxed after melting the crystals. Schick and co-workers investigated formation and relaxation of RAF in syndiotactic polypropylene, sPP, poly(carbonate), PC, and poly(3-hydroxybutyrate), PHB.[38−40] They showed[38] that the RAF in sPP formed during cooling from isothermal crystallization, as indicated by a latent heat detected in the temperature range from T_c down to T_g. The sequence length distribution of the crystallizable chains was suggested to be responsible for such behavior.[38] For PHB and PC, the RAF was established at the crystallization temperature and was relaxed at the lowest crystal endotherm.[38,39] These researchers suggested that the immobilization of the amorphous material around the less perfect crystal lamellae, which are formed during isothermal crystallization, results in forming the RAF during crystallization and relaxing the RAF during crystal melting.[38]

The existence of RAF in iPS has been demonstrated in several reports.[26,27,41,42] The amount of RAF can range from modest (10−12%) after cold crystallization[25,42] to quite large amounts (80−90%) introduced by freeze-drying iPS.[41] Our prior work[25] showed that the development of RAF with crystallization time (t_c) had a sigmoidal trend, suggesting that the RAF was formed at the same time as the crystal lamellae. Dielectric and thermal work confirmed that the amount of RAF was very small prior to spherulite impingement but increased dramatically for t_c beyond the impingement time.[42] The present work represents the first experimental study to determine both the formation and relaxation behavior of RAF in iPS. We use heat capacity measurement to confirm previous suggestions in the literature associating relaxation of RAF with the lowest temperature endotherm.[27,35,38−40,42] We show that iPS, unlike other polymers studied to date, relaxes by enthalpy involved irreversible relaxation, and in certain iPS samples RAF is the sole contributor to the lowest melting endotherm.

Theoretical Basis

In this study, we use quasi-isothermal TMDSC and standard DSC to measure the heat capacity of iPS. The basic mechanism of quasi-isothermal TMDSC expresses the time dependence of temperature as the sum of a constant term and a modulation term through[43]

$$T(t) = T_0 + A\sin(\omega t - \theta) \tag{1}$$

where T_0 is the chosen constant temperature, A is the amplitude of temperature oscillation, ω is the modulation frequency, and θ is the phase shift with respect to the reference.

The heat capactiy measured in quasi-isothermal TMDSC is the "reversing heat capacity", a term defined in TMDSC to extract a heat effect which can be reversed within the temperature range of the modulation.[43] The reversing heat capacity data collected in TMDSC system are calculated by the following equation:[44−46]

$$|mc_p + C_s - C_r \pm \Delta C_{cell}| = (A_T/A)[(K/\omega)^2 + C_r^{\,2}]^{1/2} \tag{2a}$$

$$= K'(A_{HF})/A \tag{2b}$$

where mc_p is the heat capacity of a sample of mass, m, and specific heat capacity, c_p; C_s is heat capacity of the sample pan, and C_r is the heat capacity of an empty reference pan; ΔC_{cell} is the cell asymmetry correction which can be determined by running a series of empty pans with various mass differences compared to the reference. In a later section we will outline the procedure to determine the cell asymmetry correction. On the right-hand side of eq 2, A_T is the amplitude of temperature difference between sample and reference, A is the sample temperature modulation amplitude, K is Newton's law calibration constant which is independent of modulation frequency and reference, A_{HF} is the heat flow amplitude, and K' is a calibration constant at each individual temperature provided the same experimental conditions are maintained to ensure the same heat transfer (e.g., same reference, same modulation frequency).

The total heat capacity, which consists of reversing and nonreversing components, can be obtained from a standard DSC measurement with a constant applied heating rate, q, from

$$mc_p = K''\mathrm{HF}/q \tag{3}$$

where K'' is a calibration constant and HF is heat flow. If the heat capacity is reversing, eqs 2 and 3 give the same result; if not, the difference between eqs 3 and 2 gives the nonreversing heat capacity component. In this work, both the quasi-isothermal TMDSC and standard DSC were applied to study cold-crystallized iPS. The reversible heat effect was obtained from below the glass transition to above the crystal melting point.

Experimental Section

Sample Preparation. Isotactic (90%) polystyrene powder with a weight-average molecular weight of 400 000 g/mol was obtained from Scientific Polymer Products, Inc. The powder of iPS was compression-molded at 250 °C for 3 min and then quenched into cold water to obtain the amorphous bulk films. These films were isotropic when observed between crossed polarizers. The amorphous samples were isothermally cold crystallized in a Mettler FP90 hot stage by heating them to

Table 1. Crystalline, Mobile Amorphous, and Rigid Amorphous Fractions According to Two- or Three-Phase Model Assumption for Cold-Crystallized iPS

model	ϕ_c (%)	ϕ_{MAF} (%)	ϕ_{RAF} (%)
	170 °C, 4 h		
two-phase	40	60	0
three-phase	40	50	10
	140 °C, 12 h		
two-phase	33	67	0
three-phase	33	54	13

170 or 140 °C and holding for 4 or 12 h, respectively, until crystallization was complete. The samples crystallized at T_c = 170 °C had higher crystallinity than the ones crystallized at T_c = 140 °C. Wide-angle X-ray diffraction and DSC results indicate very comparable degrees of crystallinity.[25] The crystalline fractions, ϕ_c, are listed in Table 1.

Analysis Methods. A TA Instruments temperature-modulated DSC (TA 2920 MDSC) was used for all the measurements. Cooling was accomplished by a TA Instruments liquid nitrogen cooling accessory (LNCA). The dry nitrogen gas was purged into the TMDSC cell with a flow rate of 20 mL/min. The temperature of the TMDSC instrument was initially calibrated in the standard DSC mode by using the onset of the melting peak for indium at a heating rate of 10 °C/min. Heat flow amplitude calibration was accomplished by both standard DSC and quasi-isothermal TMDSC. A 27.25 mg sapphire standard was used to determine the calibration constants K' and K'' in eqs 2 and 3. The sapphire, indium, and iPS were encapsulated in Al pans. In our thermal analysis figures, the heat flow endotherms are presented with downward deflection from the baseline.

Total Heat Capacity Measurements (Standard DSC). The standard DSC was carried out with a heating rate of 10 °C/min from room temperature to 250 °C. Three runs were taken to determine the sample heat capacity. The first run is empty Al sample pan vs empty Al reference pan to obtain baseline correction. The second run is sapphire standard vs empty Al reference pan to calibrate heat flow amplitude according to eq 3. The third run is sample vs empty Al reference pan. The same empty Al reference pan (m = 20.74 mg) was used in all the runs, and all the Al sample pans were kept the same in weight. The sample mass was kept at about 5 mg.

Reversing Heat Capacity Measurements (Quasi-Isothermal TMDSC). The reversing heat capacity measurement also consisted of three runs. The first run is empty Al sample pan vs empty Al reference pan to obtain the cell asymmetry correction. The second run is sapphire standard vs empty Al reference pan to calibrate heat flow amplitude according to eq 2. The third run is sample vs empty Al reference pan. As before, the same empty Al reference pan (m = 20.74 mg) was used in all the runs, and all the Al sample pans were kept the same in weight (m = 20.74 mg). The Al sample pan was over weighted by 2 mg compared to the reference pan to maintain the same cell asymmetry (Δm = 2 mg). The quasi-isothermal TMDSC procedure was carried out over the temperature range of 80−270 °C with a stepwise temperature increase from 2 to 3 °C, depending on the changes of heat capacity in the specific temperature range.

Figure 1 shows a quasi-isothermal TMDSC run from 160 to 270 °C. The sample temperature is plotted to show the increment of T_0 in the time domain. Because of the limited capacity of liquid nitrogen in our LNCA, we can only achieve 32 temperature steps of 20 min duration before exhausting the liquid nitrogen. Therefore, the whole temperature range from 80 to 270 °C was separated into two parts. Our experimental results showed that this method introduced no uncertainty. The temperature modulation amplitude is 0.5 °C, and the oscillation period is 1 min. Each quasi-isothermal run lasted 20 min, and the heat capacity at given T_0 was calculated by averaging the data points collected during the last 10 min.

Quasi-isothermal crystallization was executed under similar conditions, except the base temperature T_c was constant while time (t_c) varied. First the sample was heated to the crystallization temperature T_c, and then quasi-isothermal oscillation was applied with temperature modulation amplitude of 0.5 °C and oscillation period of 1 min. To prove that the heat capacity measurement at the final stage of crystallization is independent of the modulation frequency, a few additional cycles of data with alternative longer periods (90 or 100 s) were collected after completion of crystallization.

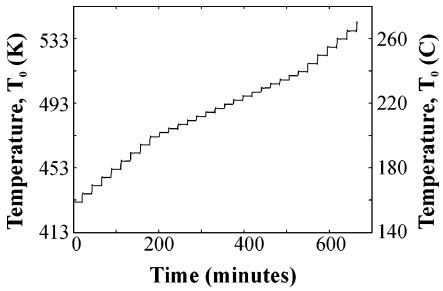

Figure 1. T_0 (K) vs time t (min) in quasi-isothermal TMDSC. Temperatures in °C are given on the right. The stepwise increment of temperature is 3 K from 433 K (160 °C) to 473 K (200 °C), 2.5 K from 473 K (200 °C) to 513 K (240 °C), and 3 K from 513 K (240 °C) to 543 K (270 °C).

Results and Discussion

Quasi-Isothermal TMDSC Cell Asymmetry. It is well-known from the heat capacity measurement in standard DSC that the heat flow of a run with identical empty pans must always be subtracted from runs with sapphire standard and samples.[47] The negative or positive deviation for the empty pans run is asymmetric, but the sign of the asymmetry in the standard DSC mode is of no concern since it has the same sign as the contribution of the identical pans used in sample and sapphire standard runs. However, under quasi-isothermal TMDSC conditions, the run of empty pans gives positive heat flow amplitude (or heat capacity) for *both* positive and negative deviations. To obtain highly precise heat capacity data, determination of the cell asymmetry must be executed, and the corresponding correction to the experimental data must be made. In the following paragraphs, we provide the method to obtain the cell asymmetry. A general solution to this problem has been suggested by the work of Schick et al.[48,49]

The following procedure was used to obtain the cell asymmetry following the work of Ishikiriyama and Wunderlich.[46] A series of empty Al sample pans with different masses were used in quasi-isothermal TMDSC runs. The equation for such runs is expressed by modifying eq 2 for the case of empty pans (m = 0) as

$$|C_s - C_r \pm \Delta C_{cell}| = (A_T/A)[(K/\omega)^2 + C_r^2]^{1/2} \quad (4)$$

The heat capacity signal was taken as the left-hand term in eq 4, and the results are plotted in Figure 2 for individual pans run under quasi-isothermal TMDSC conditions at 200 °C for 30 min. In Figure 2, the abscissa is the mass difference $\Delta m = m_s - m_r$ (in mg) between sample pan and reference pan, and the ordinate is the unnormalized heat capacity C_p (in J/K). The results for our calorimeter show that when Δm > 4.8 mg, C_p increases with increasing Δm; when Δm < 4.8 mg, C_p decreases with increasing Δm.

We define the cell asymmetry as the left-hand term within the absolute value symbol in eq 4 or

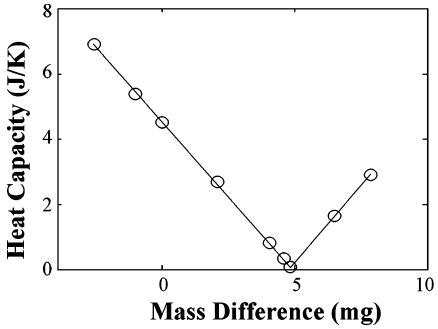

Figure 2. Quasi-isothermal TMDSC cell asymmetry. The cell asymmetry is determined by plotting the unnormalized heat capacity of empty Al sample pans vs mass difference between the reference pan and sample pan. Lines are best fits to the data.

$$C_{\text{asymnmetry}}(\Delta m) = C_s - C_r \pm \Delta C_{\text{cell}} \quad (5)$$

The TMDSC generated heat capacity can be expressed by

$$|mc_p + C_{\text{asymnmetry}}(\Delta m)| = (A_T/A)[(K/\omega)^2 + C_r^2]^{1/2} \quad (6)$$

From Figure 2 when $\Delta m > 4.8$ mg, the cell has a positive asymmetry ($C_{\text{asymnmetry}}(\Delta m) > 0$); when $\Delta m < 4.8$ mg, the cell has a negative asymmetry ($C_{\text{asymnmetry}}(\Delta m) < 0$). When the sample's total heat capacity, mc_p, is greater than the modulus of the cell asymmetry, we can write the sample measurement as

$$|mc_p + C_{\text{asymnmetry}}(\Delta m > 4.8 \text{ mg})| = mC_p + C_{\text{asymnmetry}}(\Delta m > 4.8 \text{ mg}) \quad (7a)$$

$$|mc_p + C_{\text{asymnmetry}}(\Delta m < 4.8 \text{ mg})| = |mC_p + C_{\text{asymnmetry}}(\Delta m < 4.8 \text{ mg})| \quad (7b)$$

where eqs 7a and 7b refer to either positive or negative cell asymmetry, respectively. In our experiments, for convenience we chose $\Delta m = 2$ mg (i.e., sample pan mass $m_s = 22.74$ mg and reference pan mass $m_r = 20.74$ mg). The same reference was used in all quasi-isothermal runs. Thus, a relatively small negative cell asymmetry, $C_{\text{asymnmetry}}(\Delta m = 2 \text{ mg}) < 0$, was applied compared to the total sample heat capacity. Such a configuration guarantees that the sample total heat capacity, mc_p (using samples of mass about 4 mg and sapphire standard mass 27.25 mg), was always greater than the cell asymmetry. This leads eq 7b to become

$$mC_p + C_{\text{asymnmetry}}(\Delta m = 2 \text{ mg}) = K'(A_{HF})/A \quad (8)$$

The cell asymmetry amplitude $|C_{\text{asymnmetry}}(\Delta m = 2 \text{ mg})|$ was measured by running an empty Al pan vs empty reference pan. The slope of the unnormalized heat capacity, C_p, vs Δm in Figure 2 can be used to calculate the heat capacity of aluminum at 200 °C. We obtain a value of 1.02 J/(g °C), close to the literature value for aluminum of 0.98 J/(g °C).[50]

Establishment of Steady State. The heat capacity analysis requires establishment of steady state as the basic condition.[51] The quality of steady state is especially important when the system goes through complex changes of heat capacity, e.g., glass transitions coupled with a hysteresis peak or a broad melting peak with a small amount of recrystallization.[52] The steady-state

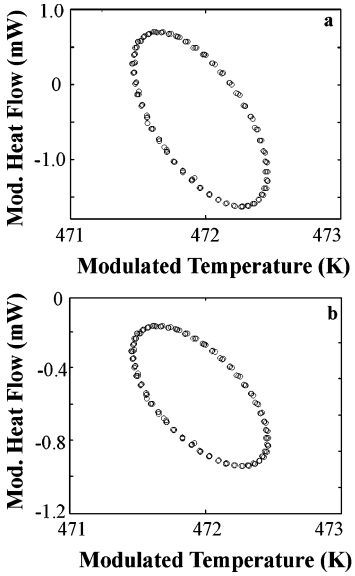

Figure 3. Modulated heat flow (mW) vs modulated temperature (K) for the last 10 min of data collection at $T_0 = 472$ K (199 °C) during quasi-isothermal TMDSC: (a) sapphire standard; (b) iPS cold crystallized at 140 °C for 12 h.

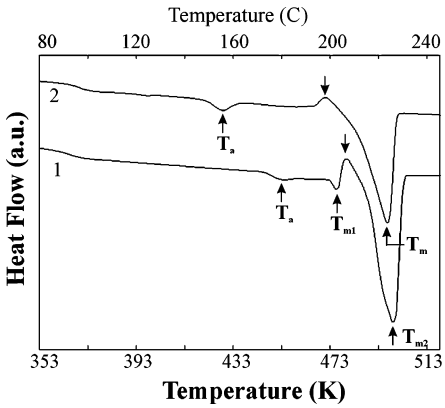

Figure 4. Standard DSC traces of iPS showing heat flow vs temperature T (K). Temperature in °C is shown at the top. IPS cold crystallized at 170 °C for 4 h (curve 1) or 140 °C for 12 h (curve 2). Endotherms are presented as downward deflections from the baseline.

condition can be verified by plotting the modulated heat flow vs modulated temperature as shown in Figure 3 for the last 10 min of a 20 min quasi-isothermal run at $T_0 = 199$ °C. Figure 3a is the sapphire standard, and Figure 3b is the iPS sample.

Both the modulated heat flow and modulated temperature are sinusoidally oscillating signals. They have the same modulation frequency, but there is a constant (nonzero) phase lag between them when the system is under the steady-state condition. Plotting one of these two signals against the other will form a Lissajous figure. As seen in Figure 3, that figure is an ellipse, and if the system is under steady state in which the phase lag is constant, each cycle of the ellipse will superimpose exactly on the previous one. Any distortion of the ellipse will indicate a corresponding distortion of the sine wave due to loss of steady state. The perfect symmetric ellipses in Figure 3 indicate the establishment of steady state during the last 10 min of the quasi-isothermal period.

Melting Behavior of iPS. Figure 4 shows the standard DSC traces of iPS cold crystallized at 170 °C

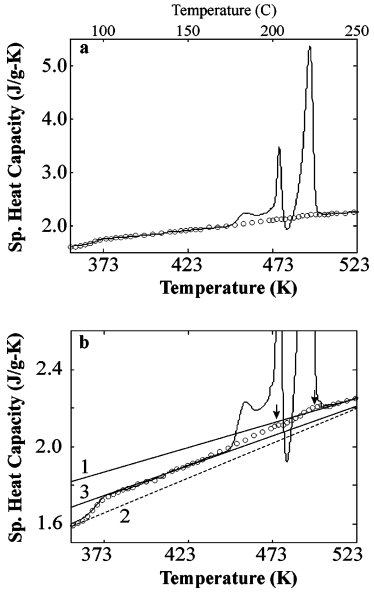

Figure 5. Specific heat capacity vs temperature obtained from both standard DSC (solid trace) and quasi-isothermal TMDSC (open circles) of iPS crystallized at 170 °C for 4 h: (a) full scaling; (b) expanded scaling. Line 1 (solid) is the heat capacity $C_p(T)|_{liquid}$ of 100% liquid, while line 2 (dashed) is the heat capacity $C_p(T)|_{solid}$ of 100% solid. These lines are obtained by using the data of the ATHAS data bank.[53] Line 3 (solid) is obtained from eq 14 based on the three-phase model, using phase fractions from Table 1. Arrows mark the locations of the peaks in the reversible heat capacity obtained from quasi-isothermal tests.

for 4 h (curve 1) and at 140 °C for 12 h (curve 2). The glass transition process occurs at about 100 °C. The endothermic (downward deflection) and exothermic peaks are marked with arrows. The first endothermic peak is termed an annealing peak, T_a, and the other higher temperature endothermic peaks at T_{m1} and T_{m2} (or, T_m, at $T_c = 140$ °C) are due to crystal melting. Just prior to the largest endotherm is a recrystallization exotherm. The impact brought by crystallization on T_a, T_{m1}, and T_{m2} has been discussed both in our earlier work[25] and in others.[27] In our current work, study of the reversibility of melting is the major objective.

Figure 5a,b shows heat capacity vs temperature during heating of cold-crystallized iPS ($T_c = 170$ °C, $t_c = 4$ h) from below T_g to the melt. Besides the quasi-isothermal TMDSC heat capacity data points (open circles), the total heat capacity (solid line) obtained by standard DSC is plotted in Figure 5a. Figure 5b is an expanded view with the heat capacity trace from standard DSC truncated. The solid line (curve 1) in Figure 5b represents the temperature-dependent heat capacity of 100% amorphous iPS (liquid) using data from the ATHAS data bank.[53] Our experimental data match the data in the ATHAS data bank extremely well, overlapping within the error limits above the melt. The other two lines in Figure 5b (curves 2 and 3) will be described later on.

Three peaks occur in the total heat capacity curve, and these are associated with the heat flow endotherms (see Figure 4, curve 1) at T_a, T_{m1}, and T_{m2} from low temperature to high temperature. The heat capacity peak associated with the recrystallization exothermic heat flow peak occurs between the two uppermost endothermic events. According to Peterman,[27] the two major higher temperature endothermic peaks (at T_{m1} and T_{m2}) arise because of dual thermal stability distribution along a single macromolecular chain. The lowest temperature endothermic peak, T_a, occurs at 184 °C, or 14 °C above the crystallization temperature T_c (170 °C). Our previous work[25] and current thermal analysis confirmed the assignment of this feature as an irreversible relaxation of rigid amorphous fraction, which will be discussed later. For this crystallization temperature, the annealing peak merges into the lower temperature range of the first melting endotherm and cannot be clearly separated. In other words, the total heat capacity trace does not return to the baseline between T_a and T_{m1}.

The quasi-isothermal measurement (open circles) matches the total heat capacity measurement very well above the melting point of the highest melting crystals and below the lowest endotherm at T_a. In between, in the vicinity of the melting peaks, T_{m1} and T_{m2}, the quasi-isothermal heat capacity departs from the total heat capacity trace. The quasi-isothermal reversing heat capacity (open circles) shows a small amount of *reversible* melting contribution to *each* melting peak. Its two tiny maxima are located on the higher temperature side of their associated melting peaks ($T_{m1} = 203$ °C and $T_{m2} = 222$ °C). Arrows mark these reversible melting peaks (open circles) in Figure 5b.

During the quasi-isothermal measurement, the temperature is oscillated by ±0.5 °C about T_0, the base temperature. The highest and lowest temperature reached during oscillation, $T_0 + 0.5$ °C and $T_0 - 0.5$ °C, are still well within the melting peak of the endotherm. Referring to Figure 5a, the total heat capacity trace (solid curve) shows two positive deflections above 200 °C. These reflect the two crystal melting events in the heat flow trace of Figure 4 (curve 1) seen during scanning calorimetry. The full width at half-maximum (fwhm) of the heat capacity peaks gives $\Delta T = 3$ °C for the lower temperature peak and $\Delta T = 8$ °C for the upper temperature peak. Thus, during oscillation about T_0, the temperature stays within the range of crystal melting since the fwhm is several times greater than the modulation amplitude. Observation of two small reversible melting peaks, associated with the two crystal melting events, is interpreted to imply that the crystal nucleus remains during the cooling cycle but does not trigger any recrystallization of already melted macromolecules for temperatures within the melting region. Quasi-isothermal TMDSC observations support the view that the macromolecular nucleation is needed in addition to crystal nucleation.[8] The relationship of the dual reversing melting peaks to morphology in iPS will be discussed after the results of Figure 6 are presented.

Figure 6a,b shows the heat capacity vs temperature for iPS crystallized at lower temperature ($T_c = 140$ °C) taken under both total heat capacity measurement by standard DSC (solid line) and by quasi-isothermal reversible heat capacity measurement (open circles). As shown in the total C_p trace (solid line), the annealing peak ($T_a = 164$ °C) here is well separated from melting, and only one major melting peak, T_m, was found at temperature higher than T_a.

In Figure 6b, the solid line (1) refers to the temperature-dependent heat capacity of 100% amorphous iPS liquid using data from the ATHAS data bank[53] (which superimposes with our measured data in the melting region). Just as in the sample treated at 170 °C, the reversible heat capacity data (open circles) matched the total heat capacity data (solid line) very well below T_a

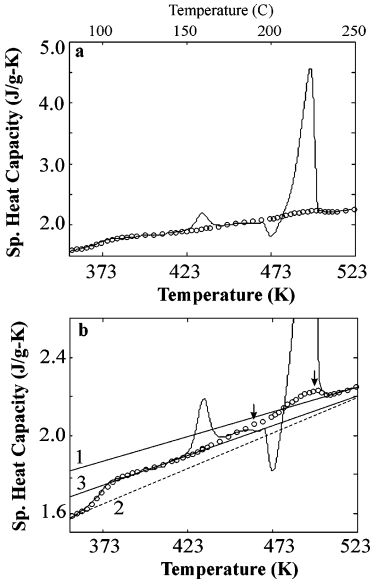

Figure 6. Specific heat capacity vs temperature obtained from both standard DSC (solid trace) and quasi-isothermal TMDSC (open circles) of iPS crystallized at 140 °C for 12 h: (a) full scaling; (b) expanded scaling. Line 1 (solid) is the heat capacity $C_p(T)|_{liquid}$ of 100% liquid, while line 2 (dashed) is the heat capacity $C_p(T)|_{solid}$ of 100% solid obtained from the ATHAS data bank.[53] Line 3 (solid) is obtained from eq 14 based on the three-phase model, using phase fractions from Table 1. Arrows mark the locations of the peaks in the reversible heat capacity obtained from quasi-isothermal tests.

and above the single upper endotherm. The reversible heat capacity trace has two small peaks located at 189 and 224 °C. The lower temperature one of these is admittedly extremely tiny, but it is reproducibly seen at the same temperature upon repeated measurement.

Within the melting region for the 140 °C sample (187−247 °C), the degree of crystallinity as a function of temperature, $\phi_c(T)$, can be calculated from[5,6]

$$C_p^{exp}(T) = \phi_c C_p(T)|_{solid} + (1 - \phi_c)C_p(T)|_{liquid} - (d\phi_c/dT)\Delta H_f(T) \quad (9)$$

$$C_p(T)|_{liquid} - C_p^{exp}(T) = \Delta H_f(T)(d\phi_c/dT) + \phi_c(d\Delta H_f(T)/dT) \quad (10)$$

where $C_p^{exp}(T)$ is the experimentally measured heat capacity, and $\Delta H_f(T)$ is the temperature-dependent heat of fusion corrected by the factor $f = 2T/(T + T_m^0)$[54] using 242 °C as the infinite crystal melting point, T_m^0.[14,27] The degree of crystallinity, shown in Table 1, is 0.33 prior to melting. The differential equation (10) was solved numerically by Euler's method (using Matlab R13). Figure 7 shows the temperature-dependent degree of crystallinity for the sample treated at 140 °C. (We did not apply the method to the 170 °C sample because the crystal melting region is overlapped by the relaxation peak at T_a.) The crystalline fraction increases slightly as temperature increases to 205 °C and then shows a gentle roll-off and decreases throughout the interval. The recrystallization exotherm (shown in Figure 6) responsible for the initial increase in crystalline fraction may be the result of repair of broken lamellae, as suggested by the TEM study of Liu and Petermann.[27]

Figures 5 and 6 show that from quasi-isothermal TMDSC we can separate the contribution of the reversing effect from the nonreversing effects shown in the total heat capacity.[1−6] In normal TMDSC, this separation was suggested initially by Reading's group.[55,56] The nonenthalpic relaxation at the glass transition, for polymers such as PET[57] and atactic PS,[58] has been analyzed by this technique. Wunderlich and co-workers applied quasi-isothermal TMDSC to study the reversible melting of polymers.[1−7] The present work shows that, similar to other linear polymers,[1−7] iPS also demonstrates a small portion of reversible melting.

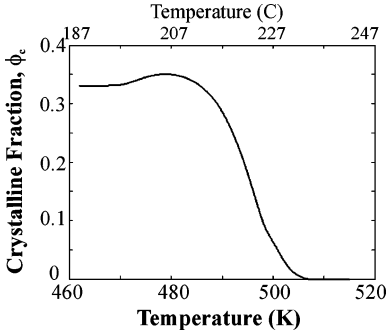

Figure 7. Crystalline fraction vs temperature obtained from eq 10 for iPS crystallized at 140 °C for 12 h.

From our current quasi-isothermal TMDSC observations, we gain further insight into iPS crystallization and melting behavior. First, the amount of reversible melting is small compared to the total DSC melting peaks, which is a typical phenomenon in long-chain macromolecules.[1−7] Second, the common explanation regarding reversible melting of macromolecules is that a portion of the molecule remains attached to higher melting crystals and cannot be separated after partial melting. This attached part was found to participate only in the high-temperature end of the melting peak.[1−9] Such a tight attachment of molecules to the crystals was suggested to be the origin of the locally reversible melting and crystallization.[8,9] Quasi-isothermal studies on iPS exhibit very similar behavior to other polymeric systems;[1−7] thus, the suggestion about a reversible melting mechanism can also apply to iPS.

Additionally, iPS treated at 170 °C shows multiple melting behavior in normal DSC studies, and the reversible melting shows also two tiny peaks, which have not, to our knowledge, been reported before in any polymer. The origin of multiple melting of iPS is due to a nonuniform thermal stability distribution along one single lamella, due possibly to uneven tacticity distribution.[27] When the temperature rises, some portion along one crystallized lamella melts first, and the rest of the lamella will melt at higher temperature. In a morphological study using TEM,[27] Petermann observed that crystal lamellae became segmented or broken, i.e., some parts melted, at a certain temperature during heating. Only later on, when the temperature continued increasing, did the other portion of the lamella melt gradually. Additionally, Petermann suggested that some of the broken lamellae became "repaired" upon further heating, and this lamellar repair may account for the recrystallization exotherm seen just before the upper melting endotherm, T_{m2}.

In quasi-isothermal TMDSC, the portion of the crystallized lamella with lower thermal stability melts first, and the molecules that are attached to these lamellae melt at the higher temperature end of the correspondent population. These portions will demonstrate locally reversible melting according to the mechanism men-

tioned above and show a tiny reversible melting peak associated with the lower temperature endothermic peak (at T_{m1}). Similarly, the same process happens to the molecules attached to the portion of lamella with high thermal stability (at high melting temperature). These molecules show their reversible melting peak in association with the higher temperature endothermic peak (at T_{m2}).

For the sample treated at 140 °C, there is only a single melting endotherm above 200 °C in the total heat capacity trace (Figure 6). We see two tiny reversible melting endotherms under quasi-isothermal conditions with the lower endotherm being very small. The fact that the lower temperature reversible endotherm is barely seen suggests that there is mostly irreversible melting in this sample at the lower temperatures. Clear reversible melting happens mostly at higher temperature, in association with the observed single endotherm. The reversible melting may refer to the same type of crystals observed, albeit at higher cold crystallization temperatures, by Liu and Petermann.[27] In studies to be reported,[59] the quasi-isothermal scan of the 140 °C sample was interrupted at 190 °C, and the sample cooled and rescanned in standard DSC. After such treatment the total heat capacity trace showed two clear peaks above 200 °C, confirming that the quasi-isothermal treatment causes dual populations of crystals to be formed. The two tiny reversible melting endotherms may result from these two different crystal populations, though the result at 140 °C is not as clear as for the 170 °C treated sample.

Heat Capacity Just above the Glass Transition. In our previous work,[25] we showed that three phases—the crystalline phase, mobile amorphous fraction (MAF), and rigid amorphous fraction (RAF)—coexist in cold-crystallized iPS. The amount of MAF, ϕ_{MAF}, was estimated by measuring the heat capacity step (ΔC_p) at the glass transition T_g.[30] The amount of RAF is then found from a three-phase assumption, where $\phi_c + \phi_{MAF} + \phi_{RAF} = 1$. For iPS samples treated at 170 or 140 °C, the amounts of RAF and MAF are listed in Table 1.

The heat capacities for both crystalline and glassy amorphous polymer are the same below T_g. Thus, at temperatures below T_g the following equality holds:

$$C_p(T)|_{crystalline} = C_p(T)|_{MAF} = C_p(T)|_{RAF} = C_p(T)|_{solid}, \quad T < T_g \quad (11)$$

When the system undergoes its glass transition, only the MAF participates in the process and above T_g the heat capacity of MAF follows the behavior of the liquid as

$$C_p(T)|_{MAF} = C_p(T)|_{liquid}, \quad T > T_g \quad (12)$$

while the other two phases (crystalline and rigid amorphous fraction) remain in the solid state. Their heat capacity relation at temperatures just above T_g will be

$$C_p(T)|_{crystalline} = C_p(T)|_{RAF} = C_p(T)|_{solid}, \quad T > T_g \quad (13)$$

The $C_p(T)|_{solid}$ was measured both by DSC and by quasi-isothermal TMDSC below T_g, and the curve was extended to higher temperature by using the data of the ATHAS data bank.[53] The $C_p(T)|_{liquid}$ was measured above the upper melting point, and the curve was extended to lower temperature by using the data of the ATHAS data bank.[53] Our experimental data of $C_p(T)|_{solid}$ and $C_p(T)|_{liquid}$ match the values listed for atactic polystyrene in the ATHAS data bank within 1.5%. The curves are shown in Figures 5b and 6b for samples treated at 170 or 140 °C, respectively. The solid line marked as curve 1 is the liquid heat capacity from $T > T_{melt}$ downward in temperature; the dashed line marked as curve 2 is the solid heat capacity from $T < T_g$ upward in temperature.

In both Figure 5b and 6b, a third curve is drawn, the solid line marked as curve 3. This curve reflects the baseline heat capacity of the semicrystalline samples above T_g where the MAF behaves as liquidlike. The meaning of the "baseline heat capacity" is that heat capacity observed in the absence of any exothermic or endothermic phase transitions that would change the phase fractions (e.g., crystallization or melting). For the semicrystalline sample, the baseline heat capacity at a given temperature, T, between T_g and T_a, is

$$C_p(T) = (\phi_c + \phi_{RAF})C_p(T)|_{solid} + (\phi_{MAF})C_p(T)|_{liquid} \quad (14)$$

There is excellent agreement between experimental data (either reversing heat capacity from quasi-isothermal measurement (open circles) or total heat capacity (solid line) from DSC) and the theoretical extrapolation using a three-phase model. In both Figures 5b and 6b, at temperatures between T_g and below the onset of the endothermic peaks, this agreement confirms the assumption of the three-phase model, with the baseline heat capacity obtained from eq 14 and phase fractions as listed in Table 1.

Formation and Relaxation of the Rigid Amorphous Fraction. In our previous work, we showed that the development of RAF at constant T_c has a similar trend to the development of crystals.[25] We suggested that RAF was forming parallel to the crystalline phase. For crystallization times prior to spherulite impingement, the rate of RAF increase is very low.[42] At longer times after impingement, RAF increases dramatically and then levels off as the crystallinity reaches its ultimate value. In the current study, we use quasi-isothermal TMDSC to observe real-time crystallization to monitor the development the crystals. From this we deduce information about the formation of RAF.

The TMDSC measurement of heat capacity has a dependence on modulation frequency. An accurate C_p measurement during quasi-isothermal crystallization at a given time requires a sufficiently high frequency, or relatively slow changes of kinetics during the measurement cycles, to avoid additional crystallization during a given cycle. A very high modulation frequency, $\nu > 100$ Hz, may be appropriate, and this should be checked independently for each polymeric system using the methodology suggested by Schick and applied initially to PC.[38−40] However, our instrumentation cannot achieve such a high frequency, and at the early stage of crystallization for iPS, the crystallization is developing on a time scale faster than the oscillation period of the TMDSC. Therefore, the technique of quasi-isothermal crystallization by TMDSC can be applied only to study the later stages of crystallization, when the crystallinity is changing only slowly compared to the oscillation period. At later stages of crystallization (i.e., $t > 120$ min for $T_c = 170$ °C or $t > 500$ min for $T_c = 140$ °C) the crystal growth rate is much slower than at the early stage.[15,25] Then, the TMDSC modulation frequency ($\nu = 1/60$ Hz) is sufficiently high compared to the rate of crystal growth. Thus, we are able to use quasi-

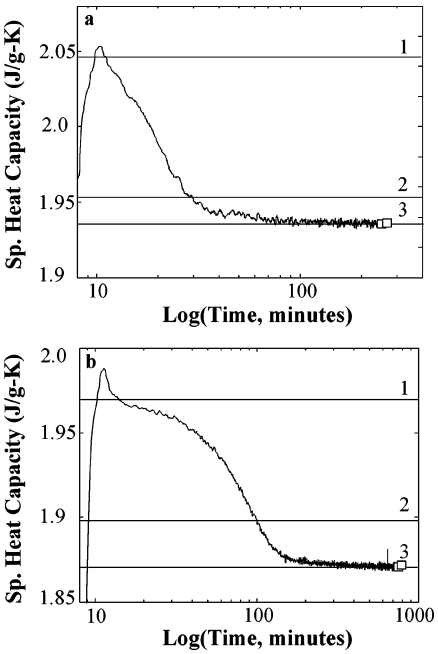

Figure 8. Specific heat capacity vs log(time) during quasi-isothermal crystallization using TMDSC with oscillation period of 60 s. IPS cold crystallized at (a) 170 °C for 4 h and (b) 140 °C for 12 h. Accurate heat capacity data are obtained only for times greater than 120 min (170 °C) or 500 min (140 °C) when crystallinity is changing only slowly. Horizontal line 1 is the heat capacity of 100% mobile amorphous at T_c; lines 2 and 3 are heat capacity calculations of the two-phase or three-phase models, respectively, at T_c, using phase fractions from Table 1. Open squares refer to measurements made at periods of 90 s (left square) or 100 s (right square).

isothermal TMDSC to obtain the heat capacity C_p at end stages of crystallization. That the measured C_p is the actual baseline heat capacity at T_c can be verified by the modulation frequency independence test suggested in refs 38−40, which we now apply to iPS.

In our current work, quasi-isothermal cold crystallization was carried out on iPS, at 170 °C (with $t_c = 4$ h) and at 140 °C (with $t_c = 12$ h). The sample was heated to the desired T_c and underwent a quasi-isothermal run with modulation amplitude of 0.5 °C and oscillation period of 60 s. The recorded data are shown in parts a and b of Figure 8 for 170 and 140 °C, respectively.

In Figure 8a,b, three horizontal lines are also drawn, labeled 1−3. Line 1 is the expected heat capacity of liquid iPS (100% amorphous) found by extending the data from the melt to the given crystallization temperature, T_c, using the ATHAS data bank.[53] Lines 2 and 3 represent the expected heat capacity of a two-phase model or three-phase model, respectively, at the completion of crystallization at temperature T_c using the respective phase fractions from Table 1. The baseline heat capacity can be expressed by

$$C_p(T) = (\phi_c + \phi_{RAF})C_p(T)|_{solid} + (1 - \phi_c - \phi_{RAF})C_p(T)|_{liquid} \quad (15)$$

In the two-phase model, we assume that no RAF forms during the crystallization, so $\phi_{RAF} = 0$ in eq 15. This is to be compared to the three-phase model, in which we assume that all RAF forms by the time crystallization is completed, at time $t|_{end}$. From Figure 8 we see that there is excellent agreement between the measured C_p (at T_c, $t|_{end}$) and that expected on the basis of the three-phase model. Such a match provides evidence that the crystalline fraction and the RAF are established at crystallization temperature T_c for a highly crystallized iPS and not during cooling.

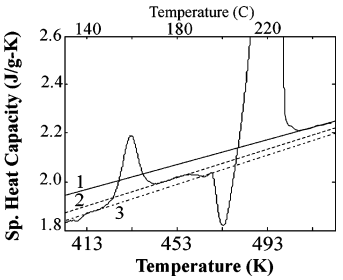

Figure 9. Specific heat capacity of iPS crystallized at 140 °C for 12 h, obtained from standard DSC from $T = 130$ °C to $T = 250$ °C. Line 1 (solid) is the heat capacity $C_p(T)|_{liquid}$ of 100% liquid, while lines 2 (dashed) and 3 (dot−dashed) are the baseline heat capacities from two- or three-phase models, respectively, using phase fractions from Table 1.

The dependence of the heat capacity measurement at $t|_{end}$ on modulation frequency was assessed. The open squares in Figure 8a,b are heat capacity measurement results which were taken at lower modulation frequency, using longer periods of 90 s ($\nu = 1/90$ Hz) or 100 s ($\nu = 1/100$ Hz), at the end of crystallization. As shown in the figure, when crystallization time t_c is greater than about 150 min for $T_c = 170$ °C (and 550 min for $T_c = 140$ °C), the crystal growth rate is quite low, and the modulation frequency is high enough to measure the accurate baseline heat capacity. This is reflected by the independence of the heat capacity measurement on frequency (open squares).

Next, we address the relaxation behavior of the RAF in iPS to demonstrate that the RAF of iPS relaxes irreversibly at T_a, the transition we called the annealing peak. From Figure 8, we found that the RAF forms at the crystallization temperature, at some time during crystallization. Indirect evidence from dielectric relaxation studies suggests that RAF forms during crystallization after impingement of crystallites.[42] Formation of RAF at T_c leads us to conclude that RAF is stable at temperatures below T_c. Furthermore, heat capacity measurements taken both by standard DSC and by quasi-isothermal TMDSC above the melting point suggest that only one phase exists at high temperature, i.e., 100% liquid (MAF). Therefore, the RAF must be relaxed at some temperature between T_c and the upper melting point. To provide further evidence for relaxation of RAF, Figure 9 shows the temperature dependent heat capacity $C_p(T)$ data for $T_c = 140$ °C and $t_c = 12$ h and for predictions based on the two-phase model (dashed curve, 2) and the three-phase model (dot−dashed curve, 3) using phase fractions from Table 1.

In Figure 9, the solid line (curve 1) is the C_p of liquid (100% MAF), the dashed line 2 is C_p according to the two-phase model (33% crystalline fraction and 67% MAF), and the dot−dashed line 3 represents the C_p according to the three-phase model (33% crystalline fraction, 13% RAF and 54% MAF). At temperatures below the annealing peak, experimental C_p matches the three-phase model. At temperature just above the annealing peak, the system approaches the two-phase model, in which only crystals and liquid (MAF) exist. Thus, as temperature increases from below T_a to above T_a, the system exhibits a transition from three-phase to two-phase, with phase fractions given in Table 1.

The association of the annealing peak with RAF, and not with the crystal phase, is based on the following observations.

1. The baseline heat capacity change, from just below ($T < T_a$) to just above ($T > T_a$) the annealing peak, results from the mobilization of a fraction of formerly rigid material equal in amount to 0.13. This amount is equal to the amount assigned to the RAF based on the $C_p(T)$ increment at T_g and the measured degree of crystallinity.

2. Using a sigmoidal baseline, we find the area of the endotherm of the annealing peak to be 2.01 J/g. With 86.6 J/g as the perfect crystal heat of fusion,[25] and 242 °C as the infinite crystal melting point, T_m^0,[14,27] we correct the heat of fusion for large undercooling by the factor, $f = 2T/(T + T_m^0)$.[54] The crystal fraction deduced in this manner from the area under the annealing peak is 0.025, which is incommensurate with the required change in baseline heat capacity at T_a.

3. Upon heating above T_a briefly, we previously found that the MAF increases (step height at T_g increases) and the annealing peak is eliminated from subsequent TMDSC scan.[25] Fourier transform infrared (FTIR) spectroscopy reveals there is no change in crystal fraction after removal of the annealing peak; i.e., the FTIR peak height ratio (PHR) of the crystalline sensitive band is unchanged.

4. Finally, the TEM observations of Liu and Petermann[27] showed that there was no change in the crystallinity, i.e., no change in the observed lamellae, when temperature T_a was just exceeded.

By all available measures (TMDSC, FTIR, TEM) there is no change in crystallinity occurring at T_a. We conclude that the observed heat capacity change occurring from $T < T_a$ to $T > T_a$ arises from the relaxation of the RAF. Thus, we confirm that the annealing peak is an irreversible relaxation of RAF, which transforms solidlike RAF into liquidlike MAF.

According to our analysis, the RAF is formed during isothermal crystallization due to strong constraints applied to the amorphous phase by the crystalline phase. RAF has a heat capacity of glassy solid state, which is not in thermodynamic equilibrium. When the RAF undergoes a heating process, the constraints exerted by the crystalline phase may be released, and this process is coupled with a production of enthalpy that leads to the annealing peak at T_a. Similar enthalpy relaxation, or structural relaxation, is seen in amorphous polymers subjected to physical aging.[60−65]

In consideration of the fact that RAF can relax to become liquidlike, and crystals can transform to the melt state, we now generalize the expression for the experimentally measured heat capacity to include these two different effects. If either the RAF is being relaxed or the crystal is being melted, the transformation is from solidlike state to liquidlike state. The melting of crystals is an enthalpy-involved process, which leads to an endothermic peak in DSC scan. Thus, in our three-phase model, according to our assumption that RAF is a solidlike state and upon our observation that the relaxation of RAF (annealing peak) shows an endothermic feature, the experimental heat capacity should be expressed by

$$C_p^{\,exp}(T) = \phi_c C_p(T)|_{solid} + \phi_{RAF} C_p(T)|_{solid} + (1 - \phi_{RAF} - \phi_c) C_p(T)|_{liquid} - (d\phi_c/dT)\Delta H_{ac}(T) + \phi_{RAF} F(T', T_{al} < T' < T_{au}) \quad (16)$$

The first three terms on the right represent the baseline heat capacity. The fourth term is the contribution from crystal melting, and the fifth term is our suggestion for the contribution from the RAF relaxation. These two terms are described below. It should be noted that in eq 16 the phase fractions ϕ_i (i = c, RAF, MAF) are all temperature-dependent quantities. Equation 16 is valid for temperatures above the glass transition of the MAF.

Regarding the fourth term in eq 16, $\Delta H_{ac} = H(\text{melt}) - H(\text{crystal})$ is the difference between the enthalpy of the melt and of the crystal. $\Delta H_{ac}(T)$ is a temperature-dependent quantity related to the heat capacity through[4,5,45]

$$d(\Delta H_{ac})/dT = C_p(T)|_{liquid} - C_p(T)|_{solid} \quad (17)$$

Regarding the last term on the right in eq 16, this term gives the contribution of the enthalpy relaxation of RAF to the experimental heat capacity and is the product of the rigid amorphous fraction, ϕ_{RAF}, and a function, $F(T')$. $F(T')$ is only nonzero in annealing peak region, and so its temperature range is restricted such that $T_{al} < T' < T_{au}$ Here, T_{al} and T_{au} are the beginning and ending temperatures of the annealing peak, respectively. The form of the function $F(T')$ is currently under investigation in our group,[59] using models of nonlinear relaxation (e.g., Narayanaswamy−Moynihan model[60−62] and Sherer−Hodge model[63−65]) that have been applied by other groups[60−65] to describe enthalpy relaxation in amorphous polymers. These studies will provide more insight into the enthalpy relaxation behavior of RAF-containing polymers.

Conclusion

Thermal analysis was carried out to determine the temperature-dependent heat capacity, $C_p(T)$, using standard DSC and quasi-isothermal TMDSC on cold-crystallized isotactic poly(styrene). The quasi-isothermal TMDSC results at high temperature suggest that there are two small amounts of reversible melting for fully crystallized iPS. Each small reversible melting peak is suggested to be associated with one of the two crystal populations observed by TEM.[27] The reversible melting peak is always located on the higher temperature side of its corresponding melting peak, suggesting that the most stable remaining crystals contain the molecules that reversibly melt. Whether the total heat flow trace in standard DSC will show two separate endotherms for the two populations depends on the scanning rate and the relative stability of the crystals against reorganization. In the present case, treatment at 140 °C results in imperfect crystals that display a single upper endotherm (above T_a) in the total heat flow trace.

Between the glass transition, T_g, and the first endothermic peak, T_a, the appropriate model for iPS is the three-phase model comprising crystals, rigid amorphous fraction, and mobile amorphous fraction. The crystals and RAF behave as solidlike in this temperature range. The annealing peak at T_a was confirmed to be a nonreversing, enthalpy-involved relaxation of rigid amorphous fraction, in which the RAF transforms from solid to liquid. The stability of RAF is dependent on the perfection of the crystalline phase. When the crystal is made more perfect through higher temperature cold crystallization, the RAF can only be relaxed at high temperature. Then the RAF relaxation peak at T_a merges into melting region of the crystals. On the other hand,

when the crystal is not perfect, i.e., when the cold crystallization temperature is closer to T_g, the relaxation of RAF occurs at a temperature that is well separated from the melting endotherm of the crystals. To accommodate the enthalpic relaxation of RAF, the experimentally determined heat capacity should be written in terms of the underlying linear baseline heat capacity plus the enthalpic terms relating to crystal melting and to relaxation of RAF.

Acknowledgment. The National Science Foundation, Polymers Program of the Division of Materials Research, supported this work through Grant DMR-0100646.

References and Notes

(1) Okazaki, I.; Wunderlich, B. *Macromolecules* **1997**, *30*, 1758.
(2) Ishikiriyama, K.; Wunderlich, B. *Macromolecules* **1997**, *30*, 4126.
(3) Wurm, A.; Merzlyakov, M.; Schick, C. *Colloid Polym. Sci.* **1998**, *276*, 289.
(4) Androsch, R.; Wunderlich, B. *Macromolecules* **2001**, *34*, 5950.
(5) Pyda, M.; Di Lorenzo, M.; Pak, J.; Kamasa, P.; Buzin, A.; Grebowicz, J.; Wunderlich, B. *J. Polym. Sci., Part B: Polym. Phys.* **2001**, *39*, 1565.
(6) Di Lorenzo, M.; Pyda, M.; Wunderlich, B. *J. Polym. Sci., Part B: Polym. Phys.* **2001**, *39*, 1594.
(7) Okazaki, I.; Wunderlich, B. *Macromol. Rapid Commun.* **1997**, *18*, 313.
(8) Wunderlich, B.; Mehta, A. *J. Polym. Sci., Polym. Phys. Ed.* **1974**, *12*, 255.
(9) Mehta, A.; Wunderlich, B. *Macromol. Chem.* **1974**, *175*, 977.
(10) Chung, J. S.; Cebe, P. *Polymer* **1992**, *33*, 2312.
(11) Lattimer, M. P.; Hobbs, J. K.; Hill, M. J.; Barham, P. J. *Polymer* **1992**, *33*, 3971.
(12) Wang, J.; Alvarez, M.; Zhang, W.; Wu, Z.; Li, Y.; Chu, B. *Macromolecules* **1992**, *25*, 6943.
(13) Kruger, K. N.; Zachmann, H. G. *Macromolecules* **1993**, *26*, 5202.
(14) Lemstra, P. J.; Kooistra, T.; Challa, G. *J. Polym. Sci., Polym. Phys. Ed.* **1972**, *10*, 823.
(15) Boon, J.; Challa, G.; Van Krevelen, D. W. *J. Polym. Sci.* **1968**, *A2* (6), 1791.
(16) Holdsworth, P. J.; Turner-Jones, A. *Polymer* **1971**, *12*, 195.
(17) Blundell, D. J.; Osborn, B. N. *Polymer* **1983**, *24*, 953.
(18) Jonas, A.; Russell, T.; Yoon, D. *Macromolecules* **1995**, *28*, 8491.
(19) Pelzbauer, P. J.; Manley, R. St. J. *J. Polym. Sci.* **1970**, *A2* (8), 649.
(20) Lemstra, P. J.; Kooistra, T.; Challa, G. *J. Polym. Sci., Polym. Phys. Ed.* **1974**, *12*, 1565.
(21) Overbergh, N.; Berghmans, H.; Reynaers, H. *J. Polym. Sci., Polym Phys. Ed.* **1976**, *14*, 1177.
(22) Petrillo, E.; Russo, R.; D'Aniello, C.; Vittoria, V. *J. Macromol. Sci., Phys.* **1998**, *B37* (1), 15.
(23) Plans, J.; MacKnight, W. J.; Karasz, F. E. *Macromolecules* **1984**, *17*, 810.
(24) Liu, T.; Petermann, J.; He, C.; Liu, Z.; Chung, T. S. *Macromolecules* **2001**, *34*, 4305.
(25) Xu, H.; Ince, B. S.; Cebe, P. *J. Polym. Sci., Polym. Phys. Ed.* **2003**, *41*, 3026.
(26) Brandup, J.; Immergut, E. H.; Grulke, E. A.; Abe, A.; Bloch, D. R. *Polymer Handbook*; Wiley-Interscience: New York, 1999; p VI/226.
(27) Liu, T.; Petermann, J. *Polymer* **2001**, *42*, 6453.
(28) Petermann, J.; Gohil, R. M. *J. Macromol. Sci., Phys.* **1979**, *B16* (2), 177.
(29) Lau, S. F.; Suzuki, H.; Wunderlich, B. *J. Polym. Sci., Polym. Phys. Ed.* **1984**, *22*, 379.
(30) Grebowicz, J.; Lau, S. F.; Wunderlich, B. *J. Polym. Sci., Polym. Symp.* **1984**, *71*, 19.
(31) Suzuki, H.; Grebowicz, J.; Wunderlch, B. *Macromol. Chem.* **1985**, *186*, 1109.
(32) Wunderlich, B. *Prog. Polym. Sci.* **2003**, *28*, 383.
(33) Huo, P. P.; Cebe, P. *Macromolecules* **1992**, *25*, 902.
(34) Huo, P. P.; Cebe, P. *Colloid Polym. Sci.* **1992**, *270*, 840.
(35) Lu, S. X.; Cebe, P. *Polym. Commun.* **1996**, *37*, 4857.
(36) Song, M. *J. Appl. Polym. Sci.* **2001**, *81*, 2779.
(37) Pak, J.; Pyda, M.; Wunderlich, B. *Macromolecules* **2003**, *36*, 495.
(38) Schick, C.; Wurm, A.; Mohammed, A. *Thermochim. Acta* **2003**, *396*, 119.
(39) Schick, C.; Wurm, A.; Mohammed, A. *Colloid Polym. Sci.* **2001**, *279*, 800.
(40) Schick, C.; Wurm, A.; Merzlyakov, M.; Minakov, A.; Marand, H. *Macromol. Symp.* **2001**, *165*, 83.
(41) Li, Y.; Xue, G. *Polymer* **1999**, *40*, 3165.
(42) Natesan, B.; Xu, H.; Cebe, P. *J. Polym. Sci., Polym. Phys. Ed.* **2004**, *42*, 777.
(43) Wunderlich, B.; Jin, Y. M.; Boller, A. *Thermochim. Acta* **1994**, *238*, 277.
(44) Boller, A.; Okazaki, I.; Ishikiriyama, K.; Zhang, G.; Wunderlich, B. J. *Therm. Anal.* **1997**, *49*, 1081.
(45) Pyda, M.; Boller, A.; Grebowicz, J.; Chuah, H.; Lebedev, V.; Wunderlich, B. *J. Polym. Sci., Polym. Phys. Ed.* **1998**, *36*, 2499.
(46) Ishikiriyama, K.; Wunderlich, B. *J. Therm. Anal.* **1997**, *50*, 337.
(47) Wunderlich, B. *Thermal Analysis*; Academic Press: Boston, MA, 1990.
(48) Hohne, G. W. H.; Merzlyakov, M.; Schick, C. *Thermochim. Acta* **2002**, *391* (1−2), 51.
(49) Merzlyakov, M.; Hohne, G. W. H.; Schick, C. *Thermochim. Acta* **2002**, *391* (1−2), 69.
(50) Takahashi, Y.; Azumi, T.; Sekine, Y. *Thermochim. Acta* **1989**, *139*, 133.
(51) Boller, A.; Jin, Y.; Wunderlich, B. *J. Therm. Anal.* **1994**, *42*, 307.
(52) Wunderlich, B.; Boller, A.; Okazaki, I.; Kreitmeier, S. *Thermochim. Acta* **1996**, *282*, 143.
(53) ATHAS data bank, http://web.utk.edu/~athas/databank/; Pyda, M., Ed., 1994.
(54) Hoffman, J. D.; Davis, G. T.; Lauritzen, J. I. In *Treatise on Solid State Chemistry*; Haney, N. B., Ed.; Plenum Press: New York, 1976.
(55) Reading, M.; Elliot, D.; Hill, V. L. *J. Therm. Anal.* **1993**, *40*, 949.
(56) Gill, P. S.; Sauerbrunn, S. R.; Reading, M. *J. Therm. Anal.* **1993**, *40*, 931.
(57) Okazaki, I.; Wunderlich, B. *J. Polym. Sci., Polym. Phys. Ed.* **1996**, *34*, 2941.
(58) Boller, A.; Schick, C.; Wunderlich, B. *Thermochim. Acta* **1995**, *266*, 97.
(59) Xu, H.; Cebe, P. *Macromolecules*, to be submitted for publication.
(60) Narayanaswamy, O. S. *J. Am. Ceram. Soc.* **1971**, *54*, 491.
(61) Moynihan, C. T.; Easteal, A. J.; DeBolt, M. A.; Tucker, J. *J. Am. Ceram. Soc.* **1976**, *59*, 12.
(62) Andreozzi, L.; Faetti, M.; Giordano, M.; Palazzuoli, D.; Zulli, F. *Macromolecules* **2003**, *36*, 7379.
(63) Scherer, G. W. *J. Am. Ceram. Soc.* **1984**, *67*, 504.
(64) Hodge, I. M. *Macromolecules* **1987**, *20*, 2897.
(65) Andreozzi, L.; Faetti, M.; Giordano, M.; Palazzuoli, D. *Macromolecules* **2002**, *35*, 9049.

MA035961N